Electronic Supplementary Information

MnO_2 flowery nanocomposites for efficient and fast removal of mercury(II) from aqueous solution: A facile strategy and mechanistic interpretation

Sankar Das,[a] Arnab Samanta,[a] Kanika Kole,[b] Gautam Gangopadhyay[a] and Subhra Jana[a,b]*

[a]Department of Chemical, Biological & Macro-Molecular Sciences, S. N. Bose National Centre for Basic Sciences, Block - JD, Sector-III, Salt Lake, Kolkata -700 106, India.

[b]Technical Research Centre, S. N. Bose National Centre for Basic Sciences, Block - JD, Sector-III, Salt Lake, Kolkata -700 106, India.

*E-mail: subhra.jana@bose.res.in

Materials

All chemicals were used as received. Potassium permanganate ($KMnO_4$), toluene, ethanol and hydrochloric acid (HCl) were received from Merck, India. Sodium hydroxide (NaOH) and mercuric chloride ($HgCl_2$) were obtained from Sisco Research Laboratory (SRL), India. Halloysite nanotubes (HNTs) were received from Sigma-Aldrich and (3-aminopropyl)triethoxysilane was purchased from Alfa Aesar.

Grafting of organosilane on HNTs

Anosilanes grafted halloysite nanotubes (HNTs) were carried out under nitrogen atmosphere using standard air free techniques. First, 3.0 g of HNTs was taken in a 50 mL three-necked round bottom flask containing 15.0 mL of toluene. Reaction flask was fixed with a rubber septum, condenser, thermocouple adaptor and an additional quartz sheath in which a thermocouple was inserted. The reaction mixture was then evacuated for 30 minutes under nitrogen at room temperature, followed by heated with a heating mantle. At 60^{o}C, 1.5 mL of (3-aminopropyl) triethoxysilane was injected into the reaction flask under stirring condition and refluxed for 20 h. Finally, the as-synthesized product was collected through simple filtration and washed several times with plenty of toluene and ethanol respectively. The product was then dried under vacuum at100 ^{o}C overnight.

Instruments and characterization

The surface morphology of HNTs/MnO_2 nanocomposites was observed via a field emission scanning electron microscopy (FESEM: FEI QUANTA FEG 250) and transmission electron microscopy (TEM: FEI TECNAI G2 F20-ST) after drop casting a drop of solution on a silicon wafer and a carbon coated copper grid respectively. High resolution transmission electron microscopy (HRTEM) and Energy dispersive X-ray spectroscopy (EDS) analyses were performed in the above mentioned TEM using an accelerating voltage of 200 kV. Powder X-ray diffraction (XRD) patterns were recorded on a RIGAKU MiniFlex II powder diffractometer using Cu Kα radiation with 35 kV beam voltage and 15 mA beam current. Specific surface area was determined by the BET method using nitrogen adsorption-desorption isotherms at 77 K with

3flex Micromeritics analyzer. Zeta potential was performed by Malvern Nano ZS instrument. Fourier Transform Infrared Spectroscopy (FTIR) measurements of the samples were performed in the range of 500 to 4000 cm^{-1} using JASCO FT/IR 6300. UV-visible absorption spectra were recorded at room temperature using a Shimadzu spectrometer, UV-2600 and taking the solutions in a 1 cm quartz cuvette. Inductively coupled plasma optical emission spectrometry (ICP-OES) analysis was carried out using the PerkinElmer ICP-OES instrument (PerkinElmer, Inc., Shelton, CT, USA).

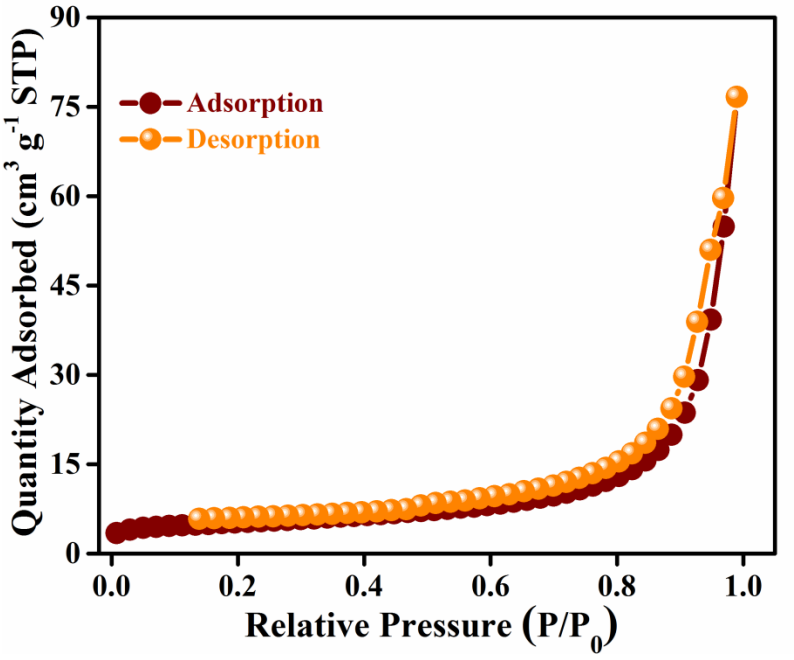

Fig. S1 The nitrogen adsorption-desorption isotherms of MnO_2 nanocomposites, signifying the formation of mesoporous materials.

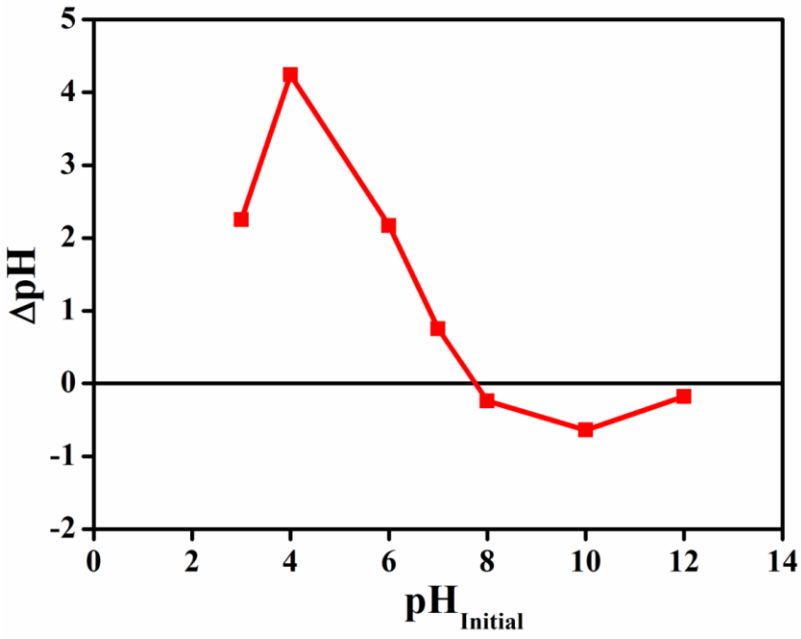

Fig. S2 pH at zero point charge (pH_{zpc}) for MnO_2 NCs. The zero point charge pH (pH_{zpc}) of the MnO_2 NCs was estimated by the pH drift method. In this method, the pH_{zpc} of the adsorbent was measured by adding 10 mL of 0.05 M NaCl solutions to several 15 mL vials and the pH of the solution was adjusted by adding HCl and NaOH aqueous solutions in the pH range of 2–12. Next, 0.03 g of the adsorbent was added to each vial and the vial was then closed properly. The suspensions was mixed well using a vortexer for 30 min and allowed to equilibrate for 48 h at ambient temperature. The suspensions were then centrifuged and the final pH values of the supernatant were measured. The value of pH_{pzc} is the point of intersection of the resulting curve at which $\Delta pH=0$.

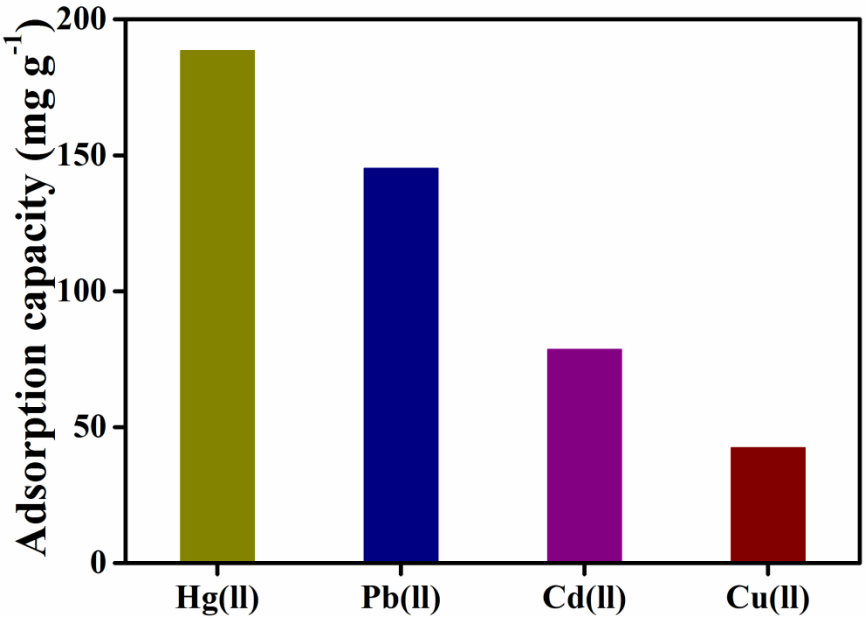

Fig. S3 Adsorption efficiencies of MnO_2 NCs for different toxic metal ions. The aqueous solution of Pb(II), Cd(II), and Cu(II) in addition to Hg(II) were taken separately with a concentration of 0.2 g L^{-1}. Then, performed the Hg(II) adsorption study keeping the concentration of the adsorbent (MnO_2 NCs) 1.0 g L^{-1}.

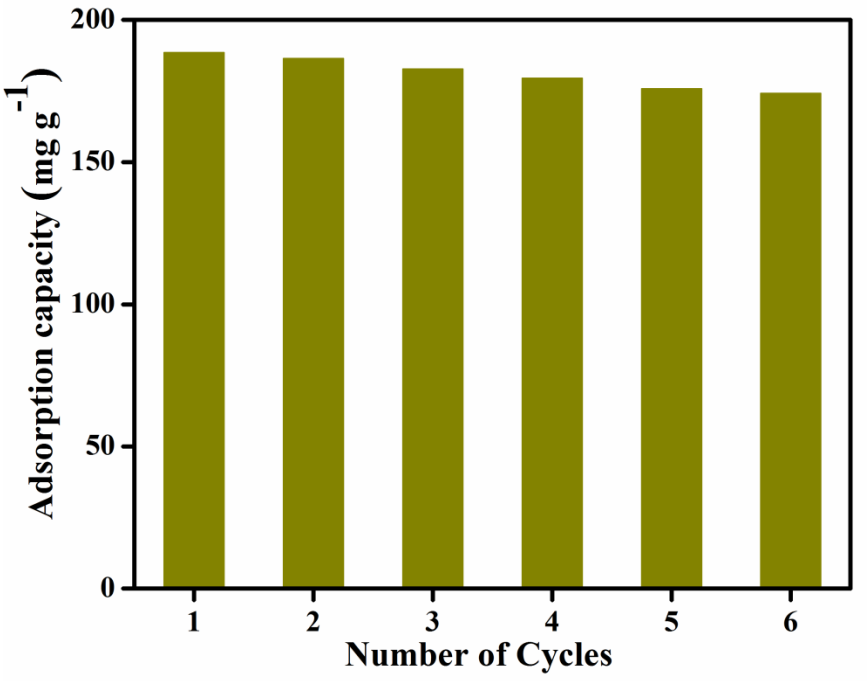

Fig. S4 Adsorption performances of MnO_2 NCs for Hg(II) ions (0.2 g L^{-1}) after multi-cycle experiments.

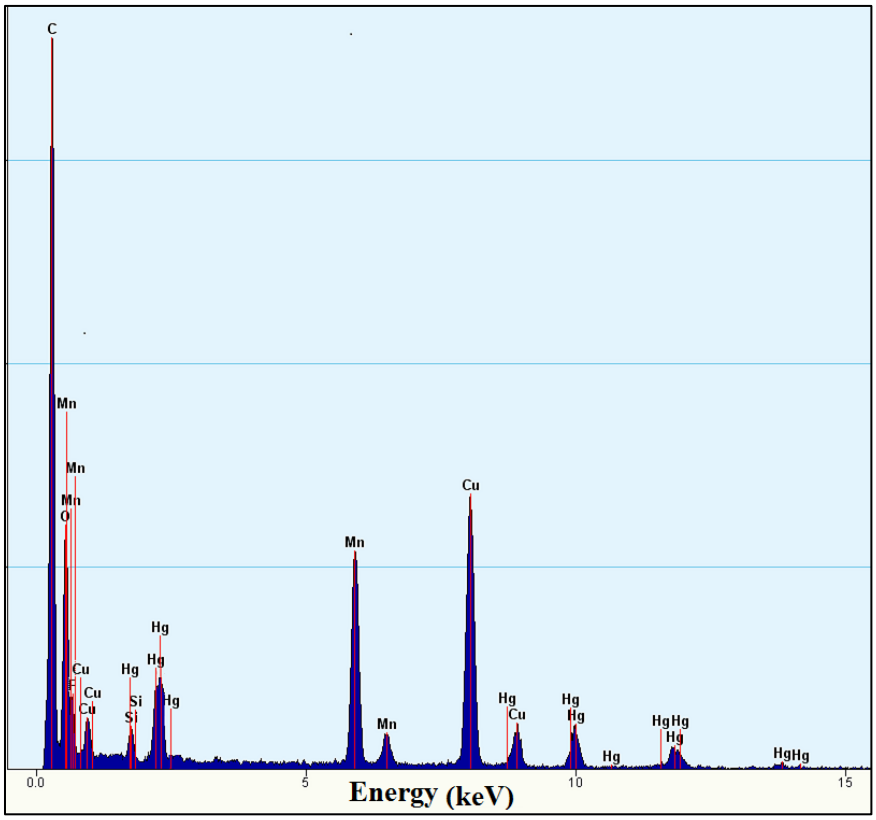

Fig. S5 EDS spectrum of MnO_2 NCs after Hg(II) sorption, demonstrating the presence of Hg with Mn and O. Signals observed for Al and Si are due to the presence of aluminosilicate clay nanotubes (HNTs). EDS spectrum was obtained after drop casting a drop of solution on a carbon coated copper grid.

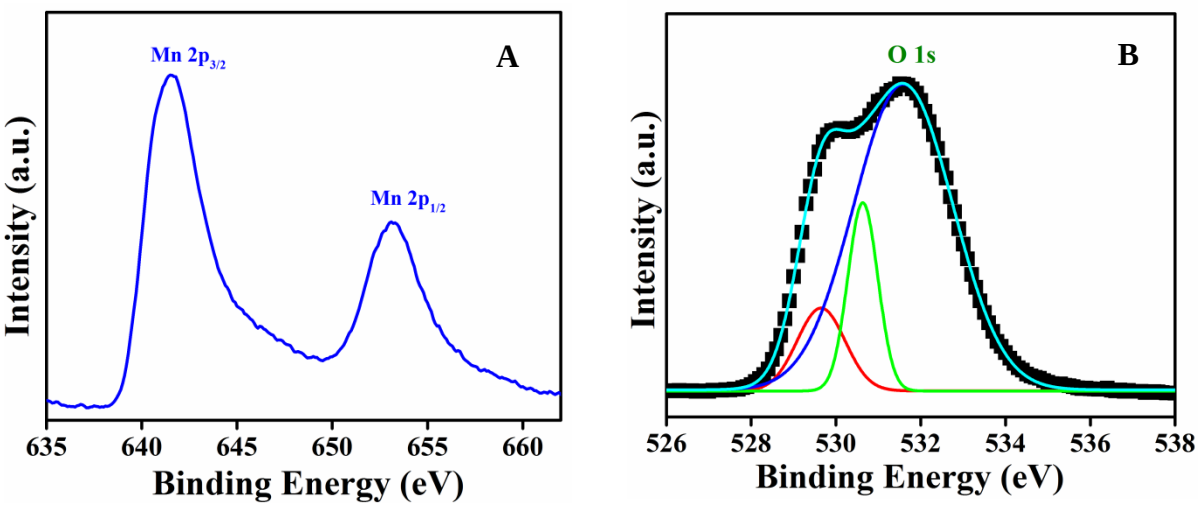

Fig. S6 XPS spectra of (A) Mn 2p and (B) O 1s region of MnO_2 NCs.

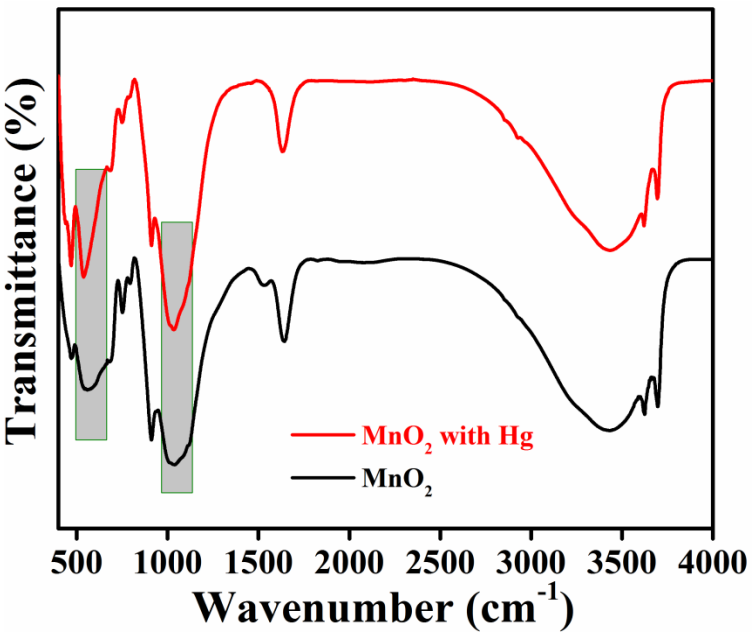

Fig. S7 FTIR spectra of MnO_2 NCs before and after Hg(II) sorption.

Table S1 Comparison of Hg(II) uptake efficacy of MnO_2 NCs with the reported oxide based adsorbents.

Adsorbents	Conc. of Hg(II) ($mg\ L^{-1}$)	Adsorption Capacity ($mg\ g^{-1}$)	References
MnO_2/CNTs	50	58.8	1
Multifunctional mesoporous microspheres (MMMs)	50	21.05	2
Thiol-functionalized CNT/Fe_3O_4	50	65.5	3
Fe_3O_4@SiO_2-SH	70	148.8	4
TiO_2 nanoparticles	75	101	5
TiO_2/Montmorillonite	75	123.8	5
Fe_3O_4-melamine based POP	180	96.92	6
Polyacrylamide-grafted iron(III) oxide	200	155	7
Nano-TiO_2	200	39.5	8
TiO_2-P25	200	100	9
TiO_2-SG	200	121	9
MnO_2 NCs	**200**	**189**	**This Work**

References

1 H. K. Moghaddam and M. Pakizeh, *J. Ind. Eng. Chem.*, 2015, **21**, 221-229.

2 C. Wang, S. Tao, W. Wei, C. Meng, F. Liu and M. Han, *J. Mater. Chem.*, 2010, **20**, 4635-4641.

3 C. Zhang, J. Sui, J. Li, Y. Tang and W. Cai, *Chem. Eng. J.*, 2012, **210**, 45-52.

4 S. Zhang, Y. Zhang, J. Liu, Q. Xu, H. Xiao, X. Wang, H. Xu and J. Zhou, *Chem. Eng. J.*, 2013, **226**, 30-38.

5 B. Dou, V. Dupont, W. Pan and B. Chen, *Chem. Eng. J.*, 2011, **166**, 631-638.

6 J. Ge, J. Xiao, L. Liu, L. Qiu and X. Jiang, *J. Porous Mater.*, 2016, **23**, 791-800.

7 G. N. Manju, K. A. Krishnan, V. P. Vinod and T. S. Anirudhan, *J. Hazard. Mater.*, 2002, **91**, 221-238.

8 Z. Ghasemi, A. Seif, T. S. Ahmadi, B. Zargar, F. Rashidi and G. M. Rouzbahani, *Adv. Powder Technol.*, 2012, **23**, 148-156.

9 M. J. López-Muñoz, A. Arencibia, L. Cerro, R. Pascual and Á. Melgar, *Appl. Surf. Sci.*, 2016, **367**, 91-100.